Supporting information

Fe, Cu dual-metal single atom catalyst on commercial carbon black for efficient oxygen reduction reaction

Hongzhou Yang,‡[a,b] He Huang,‡[a] Qing Wang,[b] Lu Shang,[,b] Tierui Zhang,[b,c] and Shouguo Wang*[,a,d]*

[a] Beijing Advanced Innovation Center for Materials Genome Engineering, School of Materials Science and Engineering, University of Science and Technology Beijing, Beijing 100083, China

[b] Key Laboratory of Photochemical Conversion and Optoelectronic Materials Technical Institute of Physics and Chemistry, Chinese Academy of Sciences, Beijing, 100190, China

[c] Center of Materials Science and Optoelectronics Engineering, University of Chinese Academy of Sciences, Beijing, 100049, China

[d] School of Materials Science and Engineering, Anhui University, Hefei 230601, China

*Corresponding authors: Lu Shang, E-mail: lushang@mail.ipc.ac.cn. Shouguo Wang, E-mail: sgwang@ustb.edu.cn.

‡ Hongzhou Yang and He Huang contributed equally to this work.

Experimental Procedures

Characterizations: Transmission electron microscope images were obtained on a HITACHI HT-7700 (HITACHI, Japan) microscope operating at an accelerating voltage of 100 kV. Aberration corrected high angle annular dark field scanning transmission electron microscope images, energy dispersive X-Ray spectroscopy elemental maps and electron energy loss spectra were obtained on an aberration-corrected JEM-ARM-300F (JEOL, Japan) transmission electron microscope operated at 300 kV. X-ray diffraction patterns were obtained on a Bruker D8 Focus X-ray diffractometer equipped with Cu Kα radiation source (λ = 1.5405 Å) operating at 40 kV. X-ray photoelectron spectroscopy (XPS) data were collected on a ESCALAB Xi+ (ThermoFisher Scientific) X-ray photoelectron spectrometer using a monochromatized Al-Kα X-ray source (hν = 1486.6 eV). X-ray absorption spectroscopy spectra were measured at the Beijing Synchrotron Radiation Facility (1W1B). Raman spectra were collected on a Renishaw inVia-Reflex spectrometer system and excited by a 532 nm laser. The metal loading contents of the SACs were measured by inductively coupled plasma optical emission spectrum (Varian 710).

Electrochemical test: CHI 760E electrochemical workstation (Chenhua Instrument, China) was used to collect electrochemical data throughout the measurement. Electrochemical measurements were performed on a standard three-electrode system with a catalyst coating glassy carbon electrode as working electrode, Hg/HgO electrode as reference electrode and platinum plate as counter electrode respectively. The working electrode was prepared by dropping catalyst ink into glassy carbon and dried in air. The

catalyst ink was prepared by mixing 4 mg catalyst powder, 480 μL isopropanol, 500 μL deionized water and 20 μL nafion solution (5 wt.% in water and 1-propanol, Alfa) together, and ultrasonicated for 1 h forming a homogeneous solution. For FeCu-SAC, Fe-SAC and Cu-SAC, 10 μL ink was dropped on polished glassy carbon electrode and the catalyst loading was 0.8 mg cm^{-2}. For commercial Pt/C, 5 μL ink was dropped on polished glassy carbon electrode and the Pt loading was 0.08 mg cm^{-2}.

Before tests, the electrolyte was first saturated by purging with O_2 or N_2 at least 30 min, and the gas flow was maintained throughout the test. For rotating disk electrode (RDE) tests, the linear sweep voltammetry (LSV) curves were measured at a scan rate of 10 mV s^{-1} in O_2 and N_2 saturated electrolyte. The final oxygen reduction current was obtained from the difference between LSV curves measured in O_2 and N_2 saturated electrolyte. Rotating ring-disk electrode (RRDE) tests were applied to measure the electron transfer number (n) and hydroperoxide yield (H_2O_2%) using the following equations:

$$n=\frac{4\times I_D}{I_D+\frac{I_R}{N}}$$

$$H_2O_2\%=\frac{200\times I_R}{I_R+N\times I_D}$$

Where I_D was the Faradaic current at disk, I_R was the Faradaic current at Pt ring, and N was the H_2O_2 collect efficiency at the ring (37 %).

DFT calculations: First-principles calculations were performed based on the density functional theory (DFT)[1] as implemented in the Vienna Ab-initio Simulation Package (VASP) by adopting the generalized gradient approximation (GGA) with the Perdew-Burke-Ernzerhof (PBE) exchange-correlation functional.[2,3] To simulate the ORR

multi-step process on the pristine Pt/C and Fe/Cu doped nitrogenated graphene (C-FeN_4/C-CuN_4), the atomic structures of 2 × 2 Pt (111) slab and 2 × 2 × 1 nitrogenated graphene anchoring with Fe/Cu or dual FeCu metal dopants were constructed, as shown in Fig. S27. The whole ORR process was divided into five elementary steps:

1) $O_2 + * \rightarrow O_2*$

2) $O_2* + H_2O + e^- \rightarrow OOH* + OH^-$

3) $OOH* + e^- \rightarrow O* + OH^-$

4) $O* + H_2O + e^- \rightarrow OH* + OH^-$

5) $OH* + e^- \rightarrow OH^- + *$

Where * indicates adsorption sites. Different intermediate adsorption configurations of *O, *OH, and *OOH on the Pt and Fe/Cu doped C-N_4 surfaces were enumerated and the most equilibrium sites were calculated. The vacuum slabs were set more than 15 Å to avoid the periodic boundary interactions.[4] Especially for the Pt (111) slab, the bottom two layers were constrained to represent the bulk property of Pt substrate.[5] To consider the van der Waals interaction for the intermediates adsorption/desorption, DFT-D3 method by Grimme et al.[6] was considered in the DFT calculations. The plane wave energy cut-off was set to 520 eV and a 3 × 3 × 1 Monkhorst-Pack k-point mesh was sampled. All structures were fully optimized until the final energy and residual force convergence reached 10^{-5} eV and 0.02 eV $Å^{-1}$, respectively. The adsorption energy of intermediates on the catalyst surface was calculated as,

$$\Delta G = G_{ad+substrate} - G_{substrate} - G_{ad}, \quad (1)$$

where the $G_{ad+substrate}$, $G_{substrate}$, and G_{ad} represent the Gibbs free energies of catalyst

surface with/without intermediates adsorption and studied intermediates, respectively. In particular, during the Gibbs free energy calculation, the zero-point energy and entropy change with the consideration of temperature effect were considered, which is defined as

$$G = E + E_{zpe} - T\Delta S, \quad (2)$$

in which E_{zpe} and $T\Delta S$ represent the zero-point energy and vibrational entropy part of the adsorptive intermediates. All energy corrections were obtained using the open-source VASPKIT package.[7]

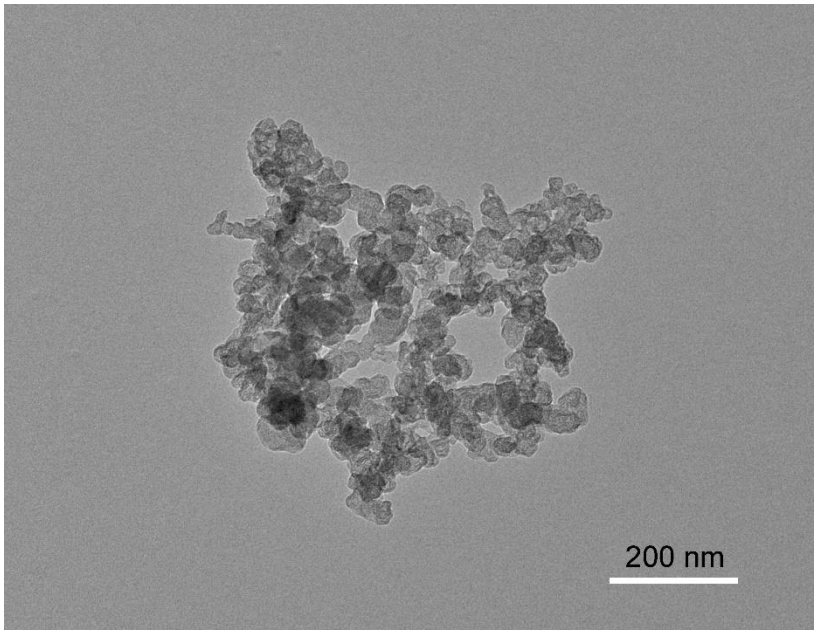

Fig. S1. TEM image for Ketjen black EC-300J.

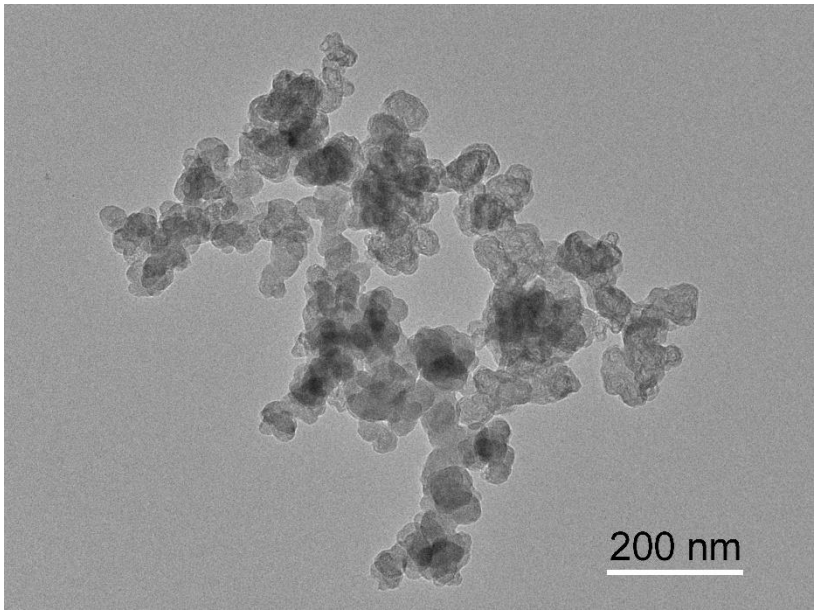

Fig. S2. TEM image for Fe-SAC.

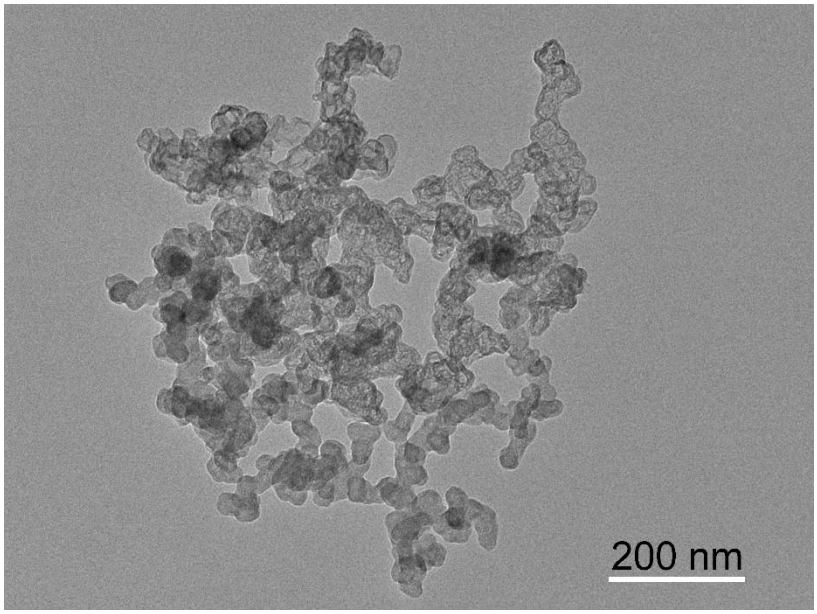

Fig. S3. TEM image for Cu-SAC.

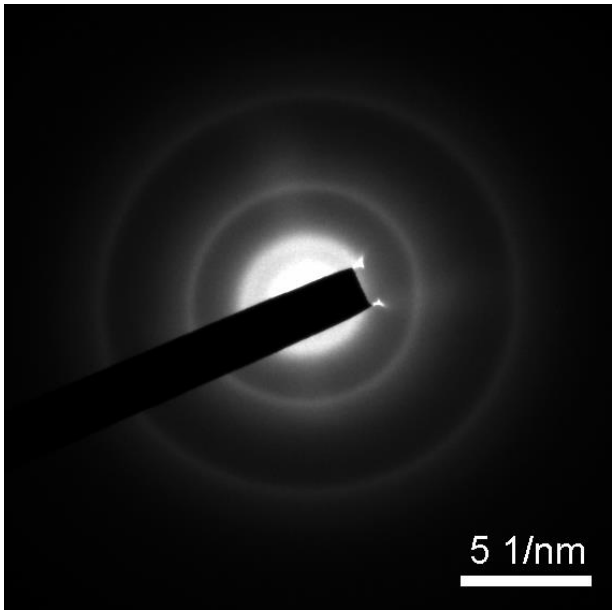

Fig. S4. SAED pattern for Fe-SAC.

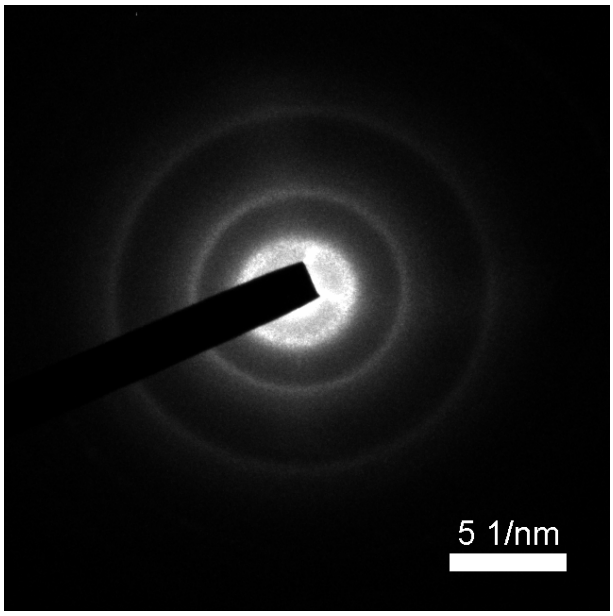

Fig. S5. SAED pattern for Cu-SAC.

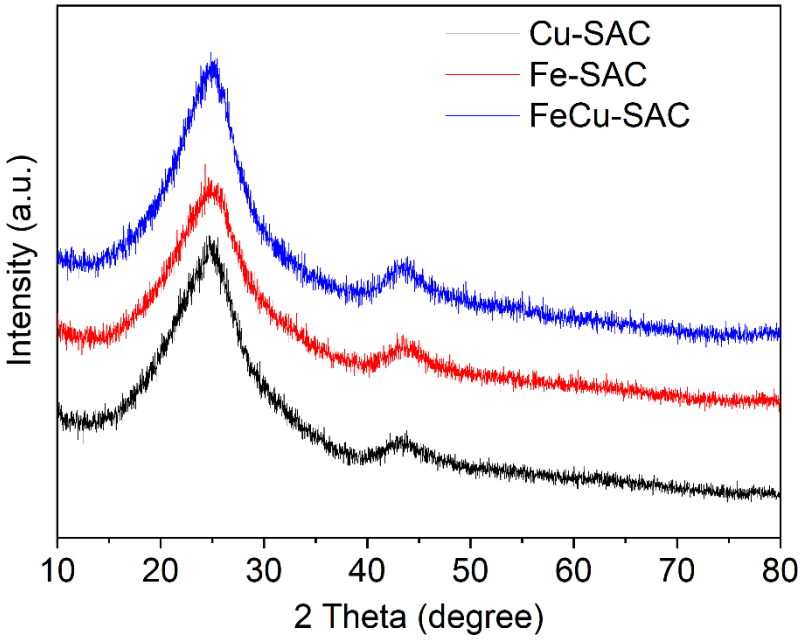

Fig. S6. XRD patterns for FeCu-SAC, Fe-SAC and Cu-SAC.

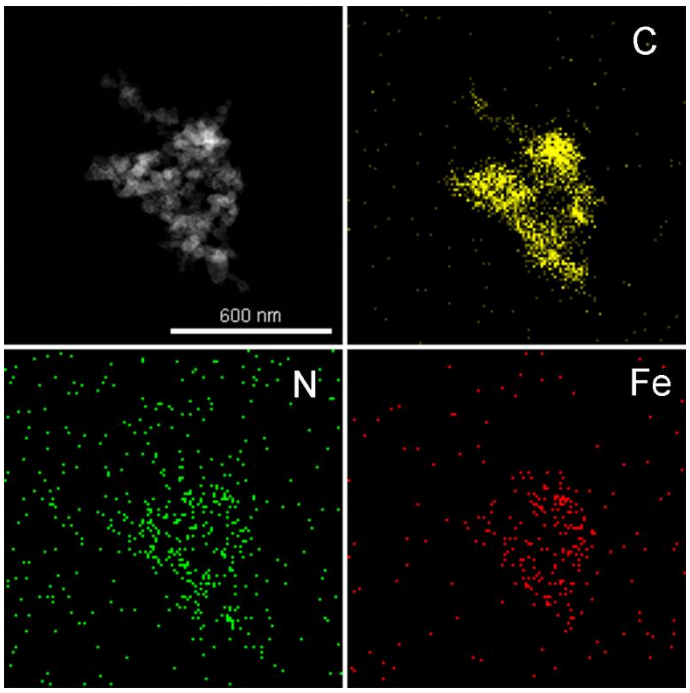

Fig. S7. EDX elemental mapping images for Fe-SAC.

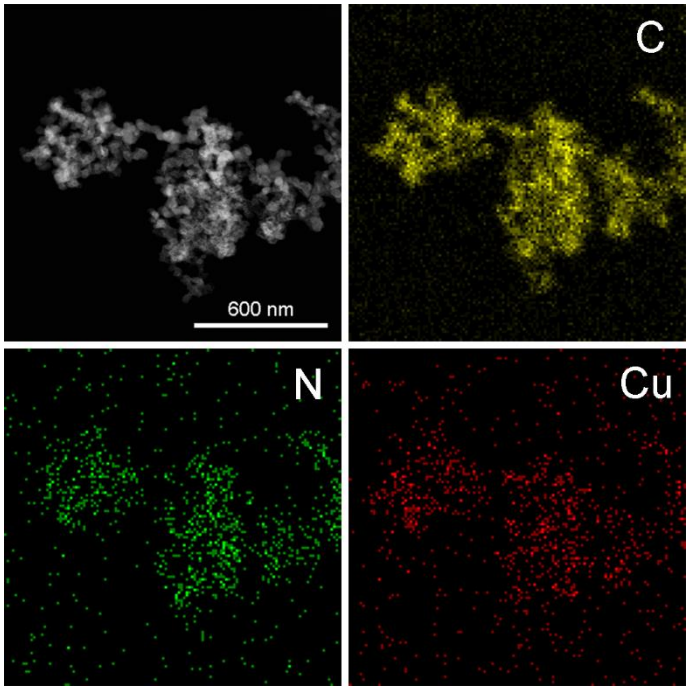

Fig. S8. EDX elemental mapping images for Cu-SAC.

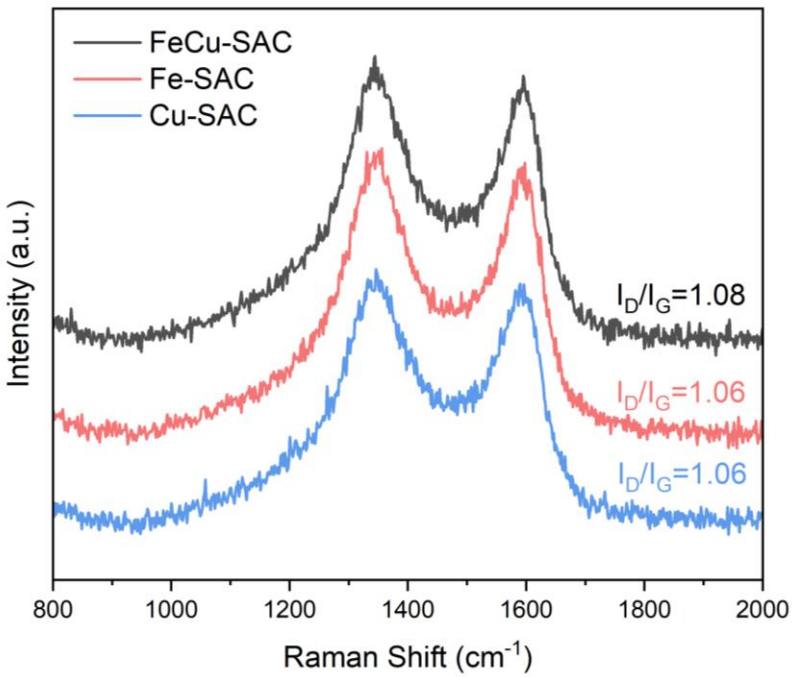

Fig. S9. Raman spectra for FeCu-SAC, Fe-SAC and Cu-SAC.

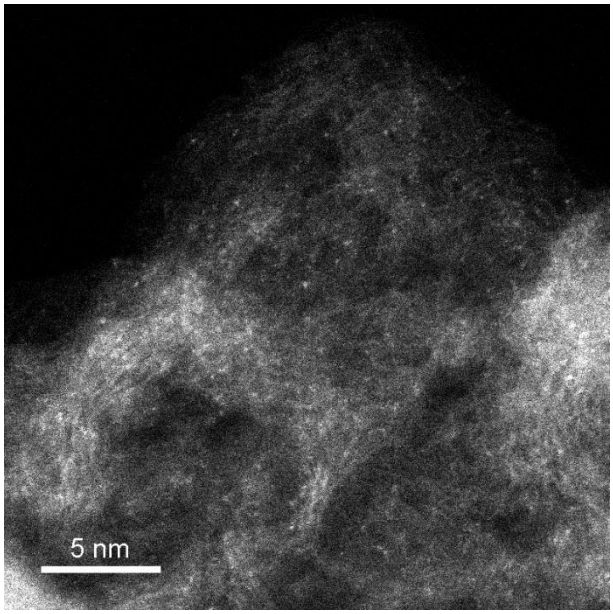

Fig. S10. HAADF-STEM image for Fe-SAC.

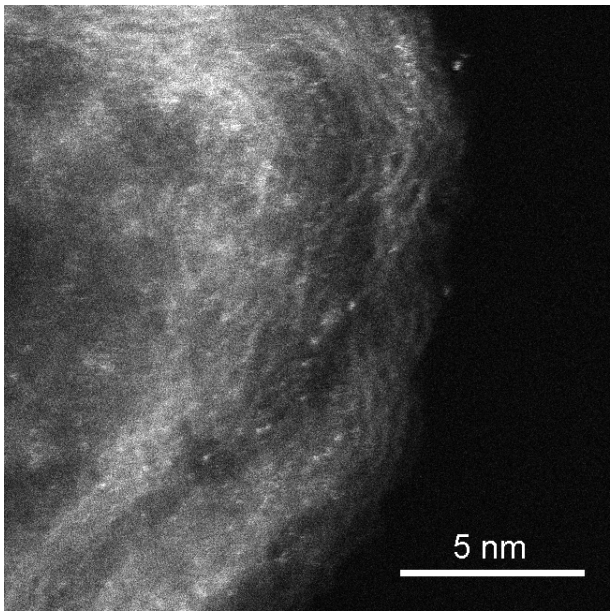

Fig. S11. HAADF-STEM image for Cu-SAC.

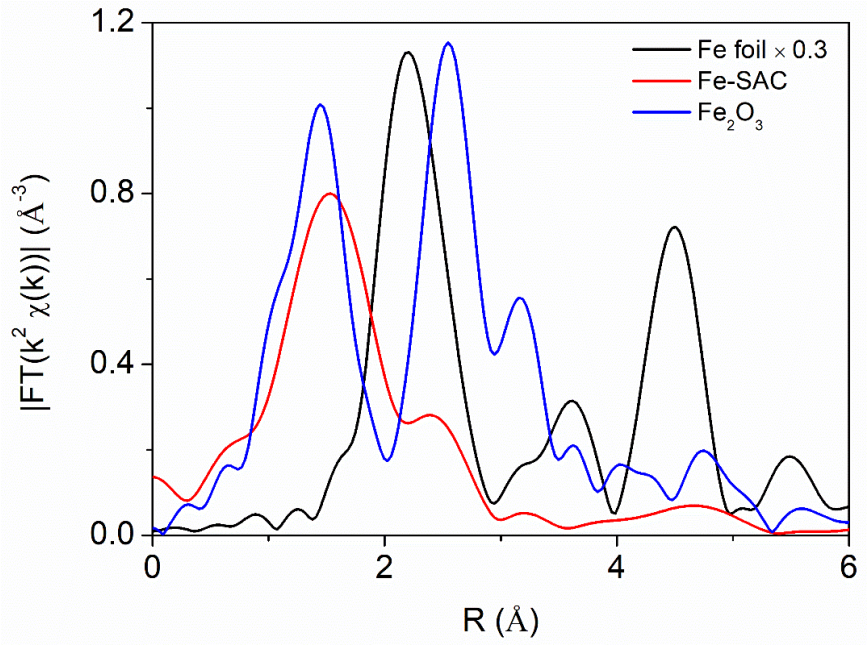

Fig. S12. EXAFS R space plots for Fe-SAC and references.

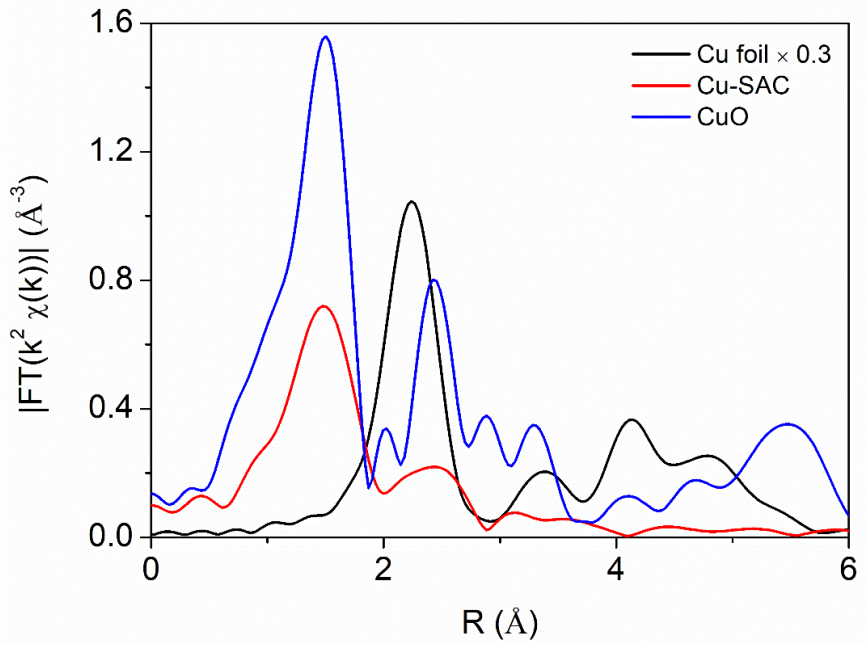

Fig. S13. EXAFS R space plots for Cu-SAC and references.

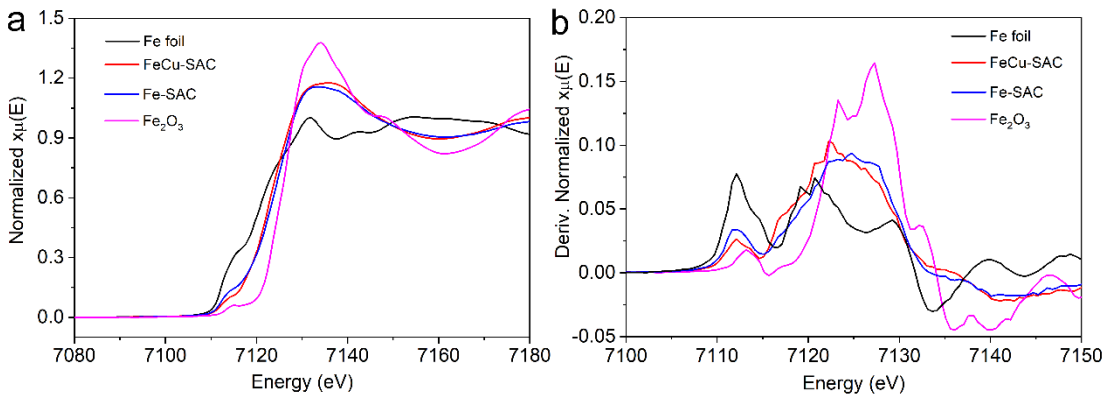

Fig. S14. XANES and first-derivative XANES plots for FeCu-SAC, Fe-SAC and references.

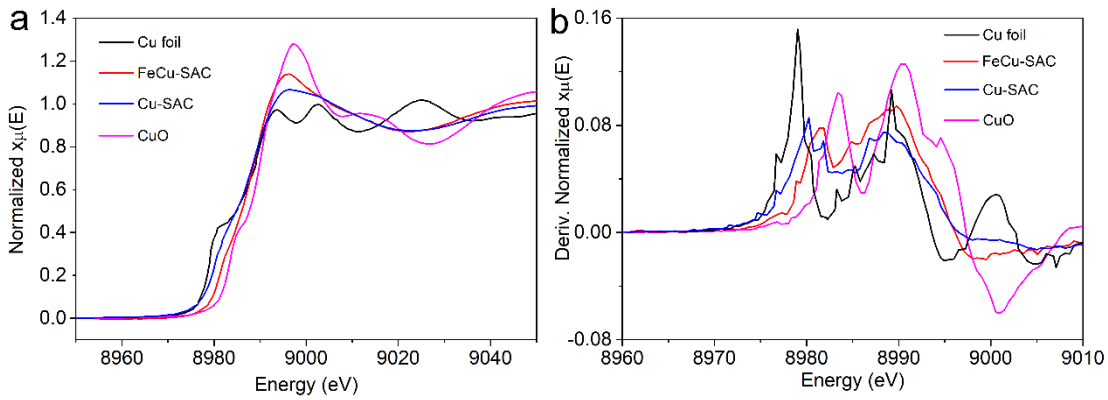

Fig. S15. XANES and first- derivative XANES plots for FeCu-SAC, Cu-SAC and references.

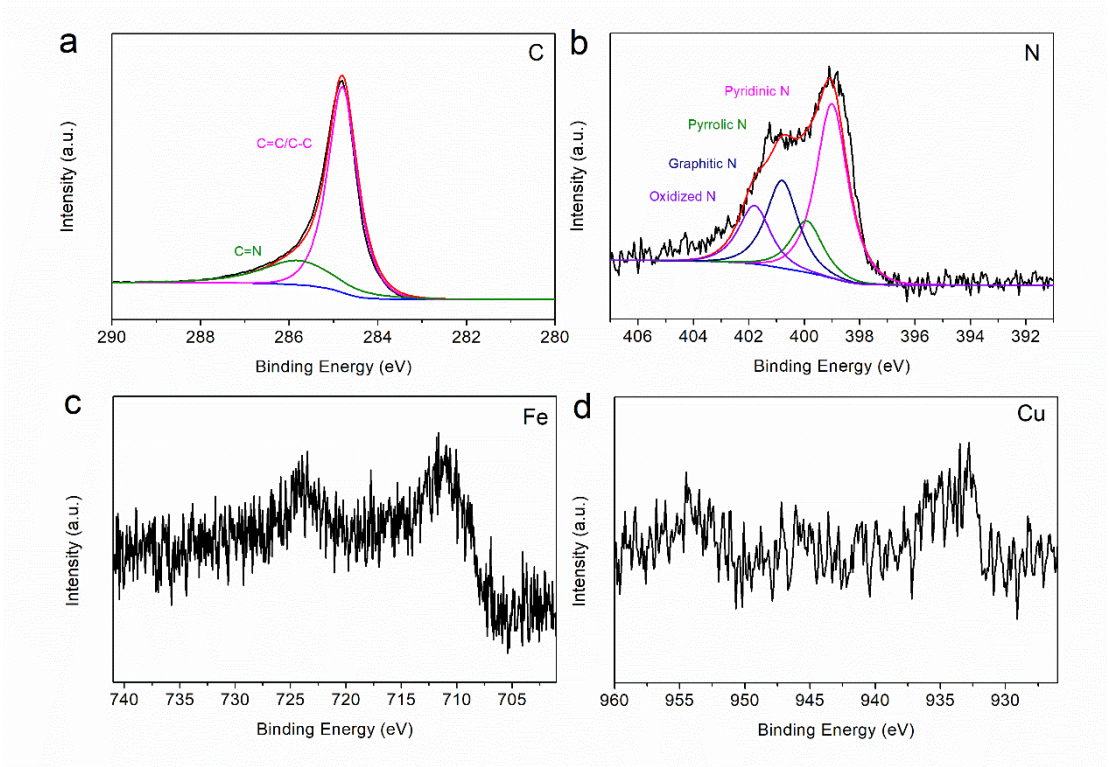

Fig. S16. XPS fine spectra for FeCu-SAC.

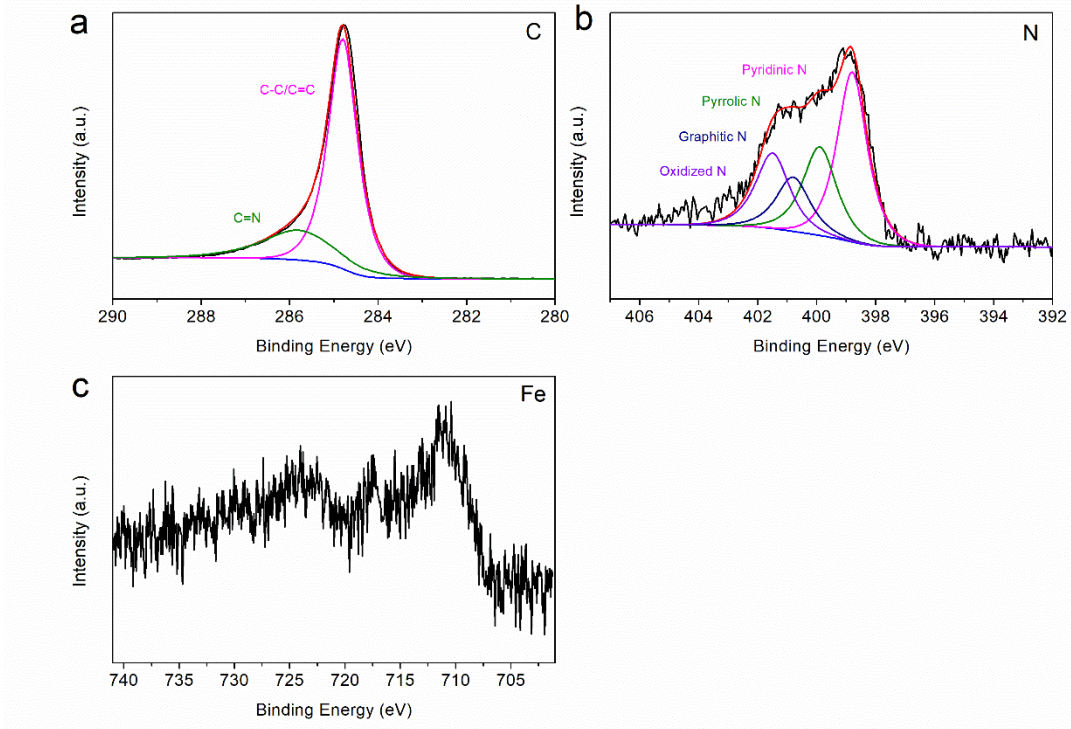

Fig. S17. XPS fine spectra for Fe-SAC.

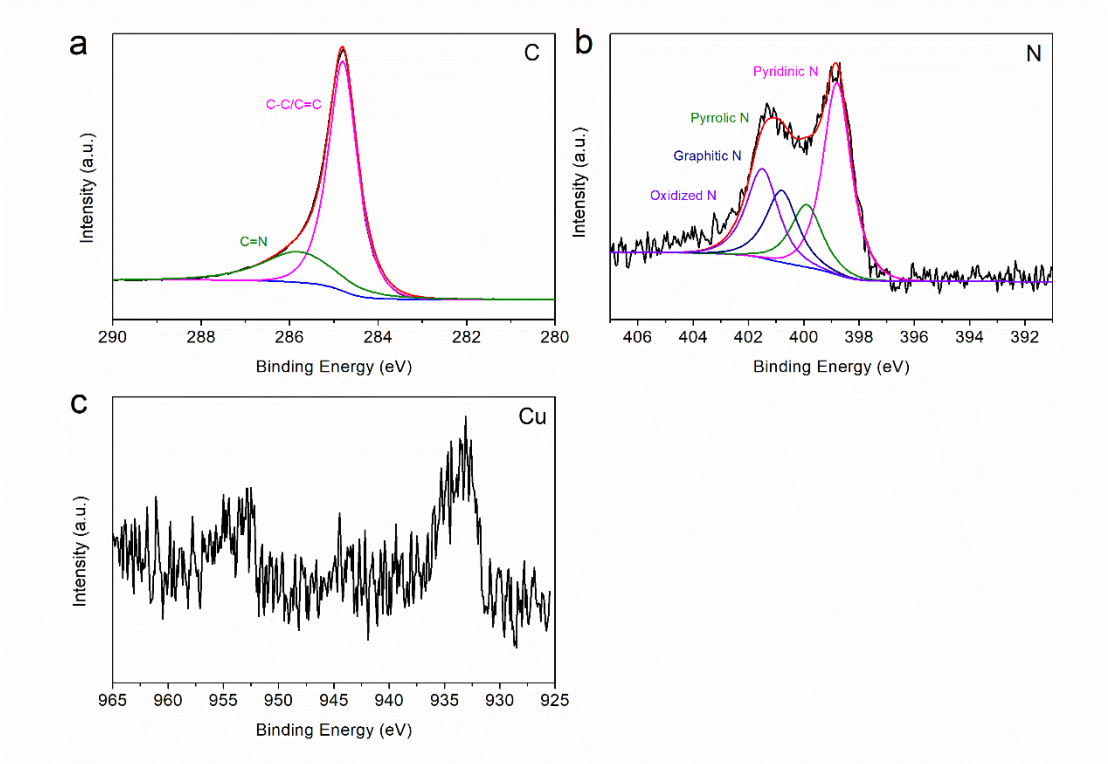

Fig. S18. XPS fine spectra for Cu-SAC.

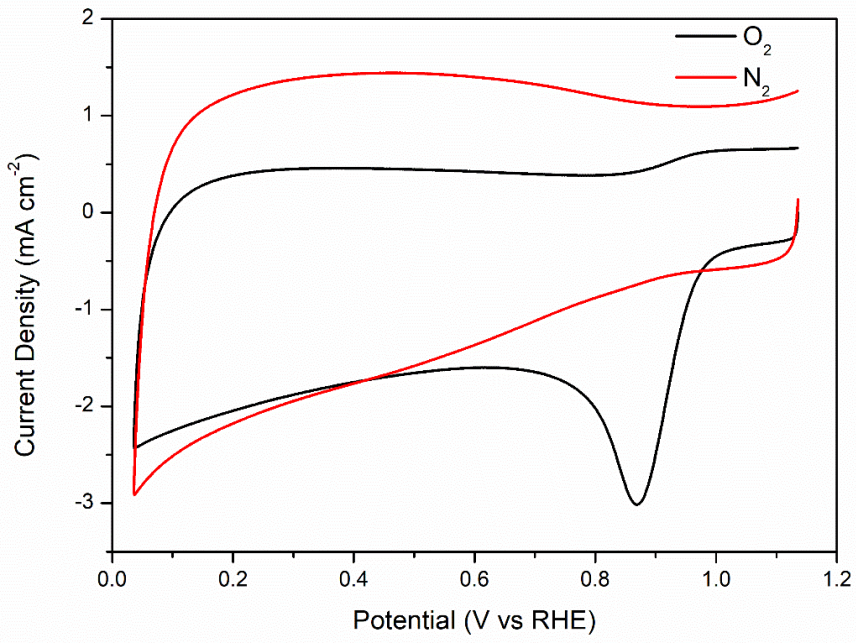

Fig. S19. CV curves of FeCu-SAC in O_2 and N_2 saturated 0.1 M KOH electrolyte.

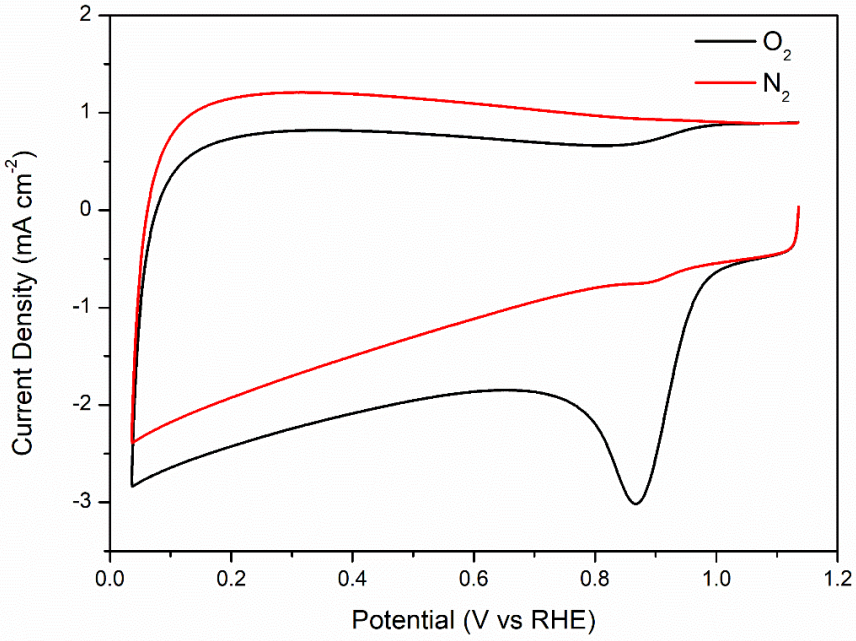

Fig. S20. CV curves of Fe-SAC in O_2 and N_2 saturated 0.1 M KOH electrolyte.

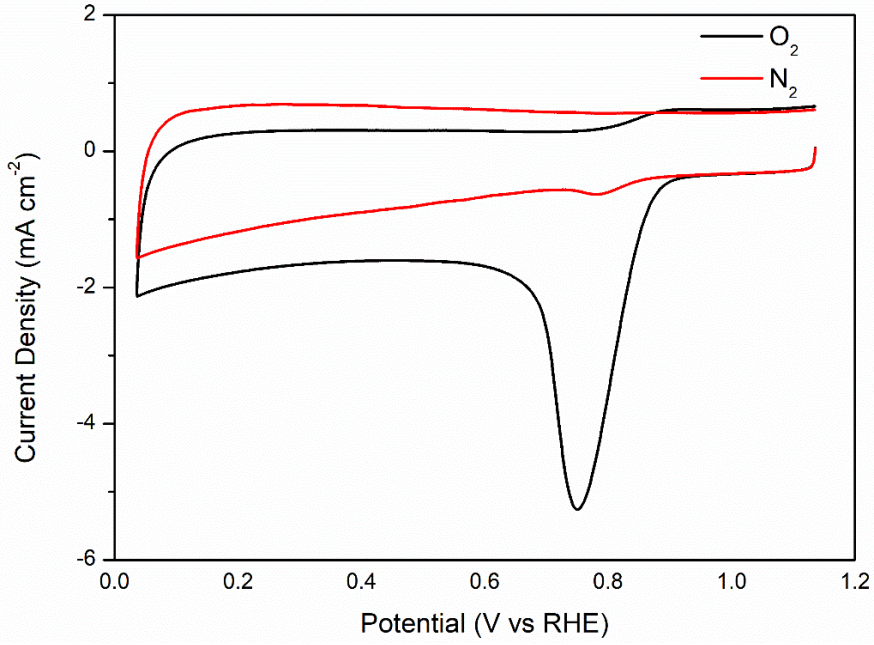

Fig. S21. CV curves of Cu-SAC in O_2 and N_2 saturated 0.1 M KOH electrolyte.

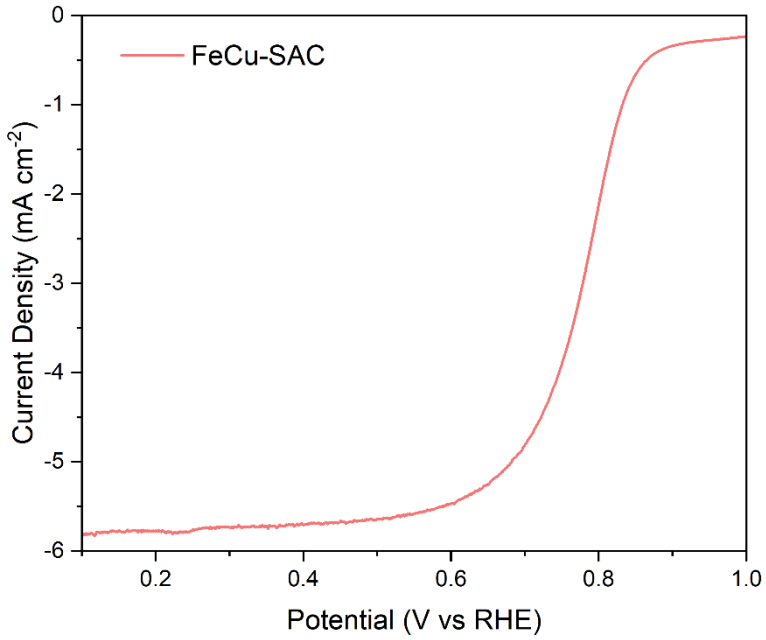

Fig. S22. ORR LSV curve of FeCu-SAC in 0.5 M H_2SO_4.

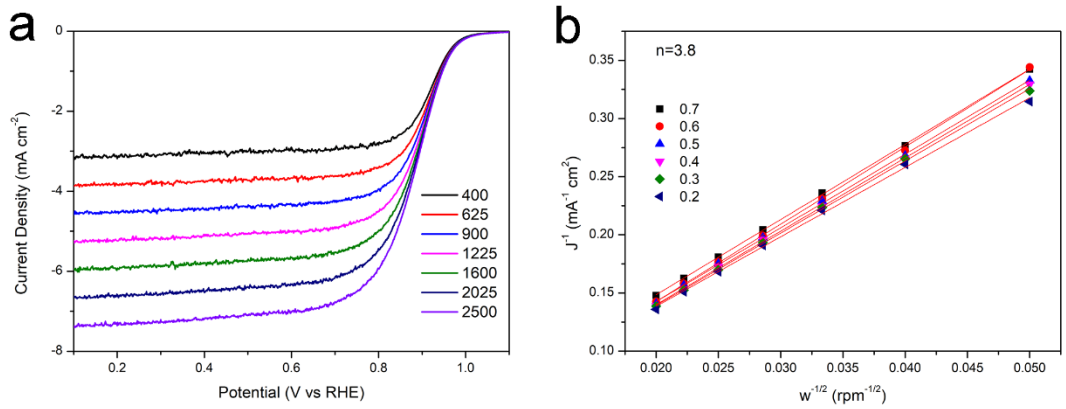

Fig. S23. ORR LSV curves and derived K-L plots of FeCu-SAC.

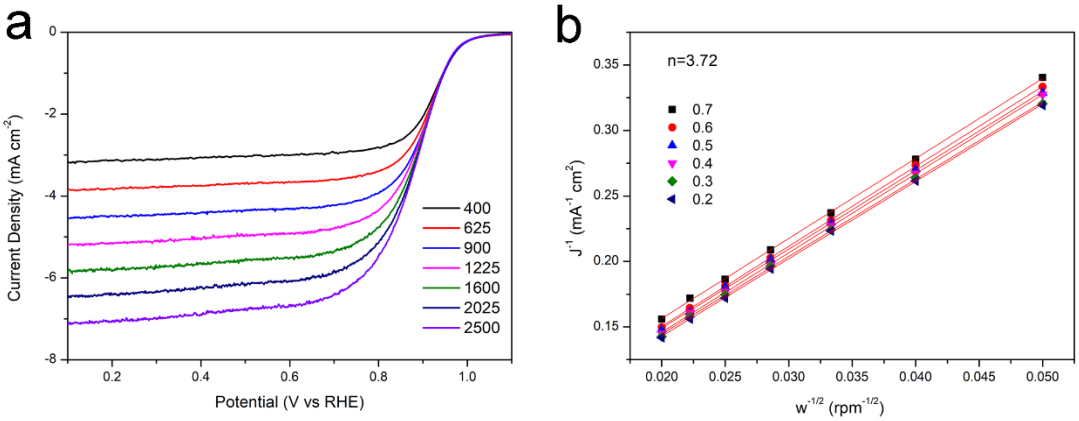

Fig. S24. ORR LSV curves and derived K-L plots of Fe-SAC.

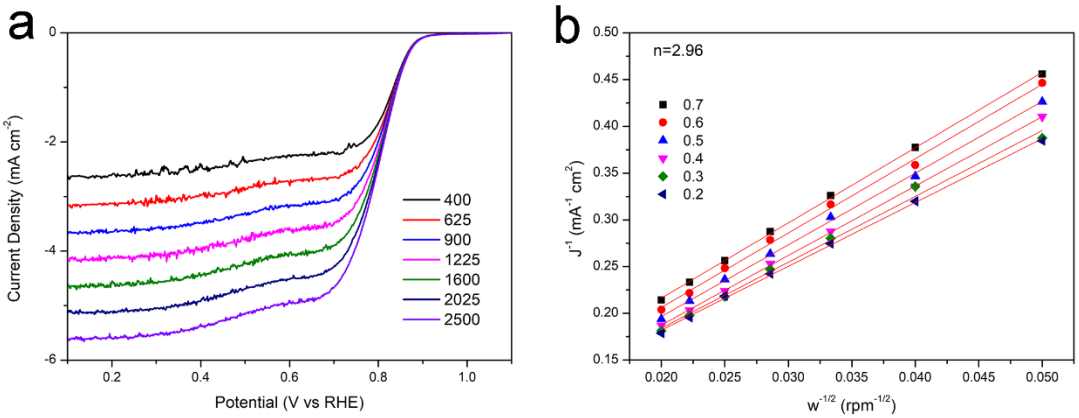

Fig. S25. ORR LSV curves and derived K-L plots of Cu-SAC.

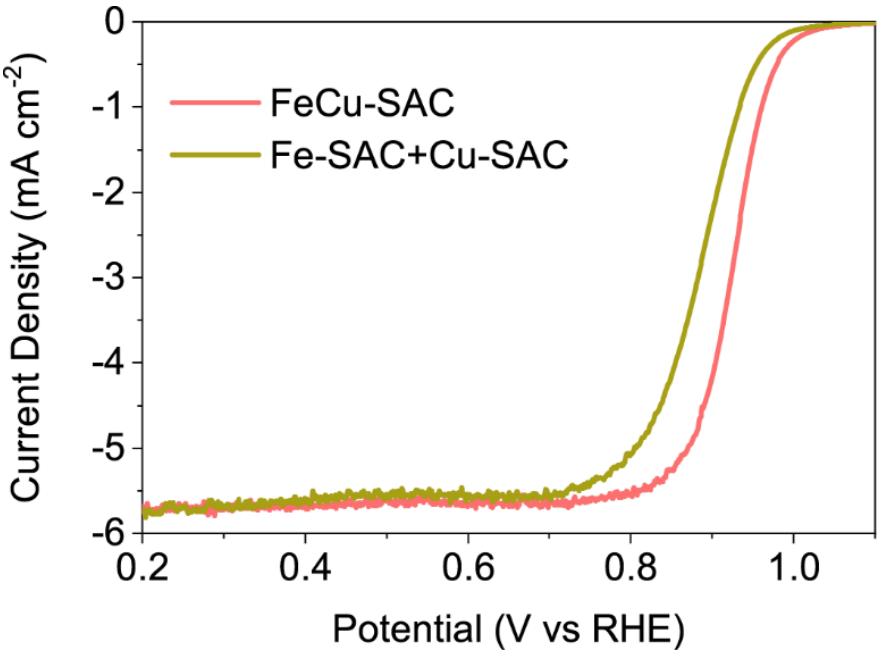

Fig. S26. ORR LSV curves of FeCu-SAC and physically mixed Fe-SAC + Cu-SAC.

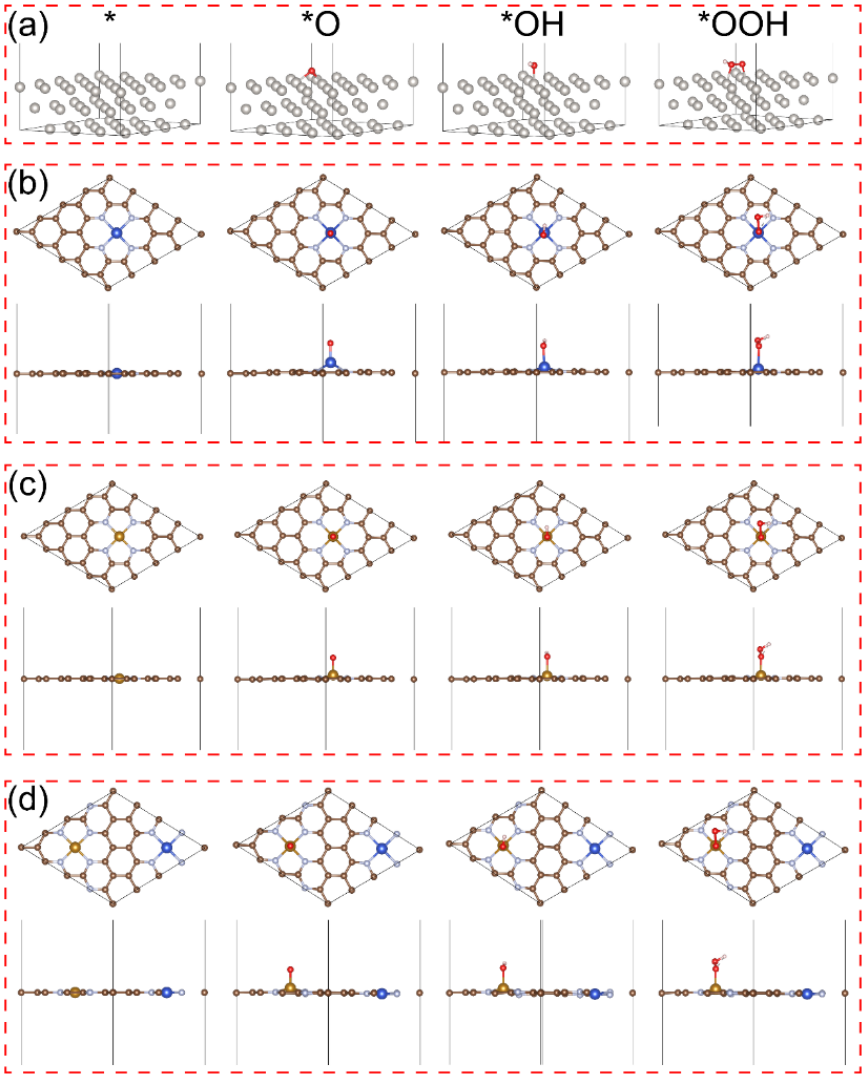

Fig. S27. Optimized structure revolution for ORR on (a) Pt (111) slab, (b) Cu-SAC, (c) Fe-SAC, and (d) FeCu-SAC. The silver, brown, white, yellow, blue, red and pink balls represent Pt, C, N, Fe, Cu, O, and H atoms, respectively.

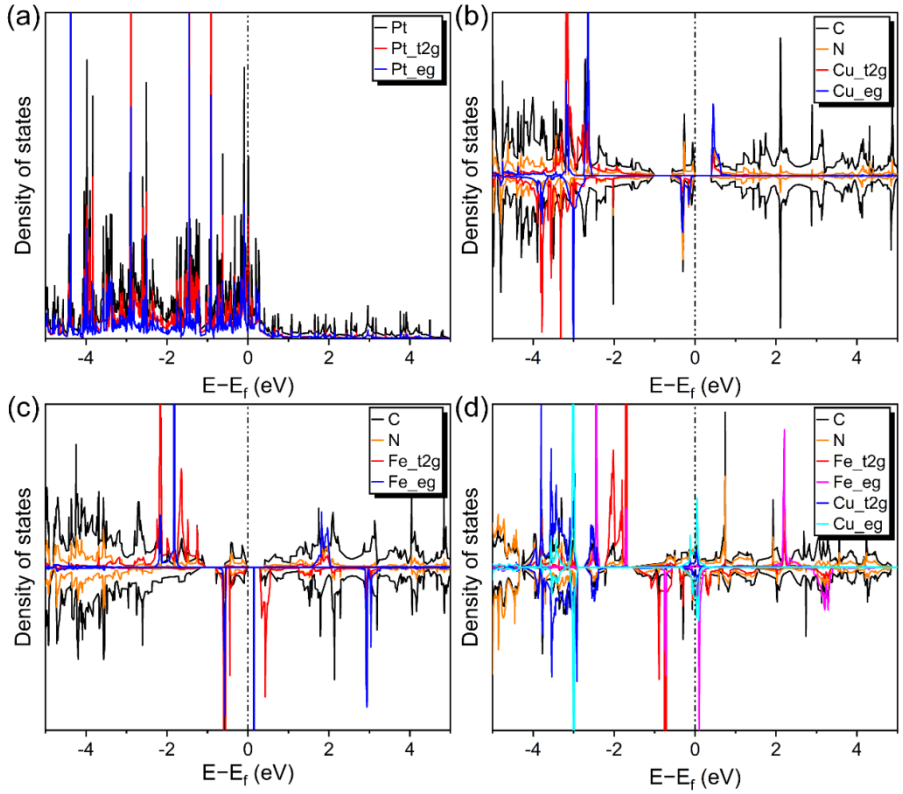

Fig. S28. Partial electronic density of states of (a) Pt (111) slab, (b) Cu-SAC, (c) Fe-SAC, and (d) FeCu-SAC.

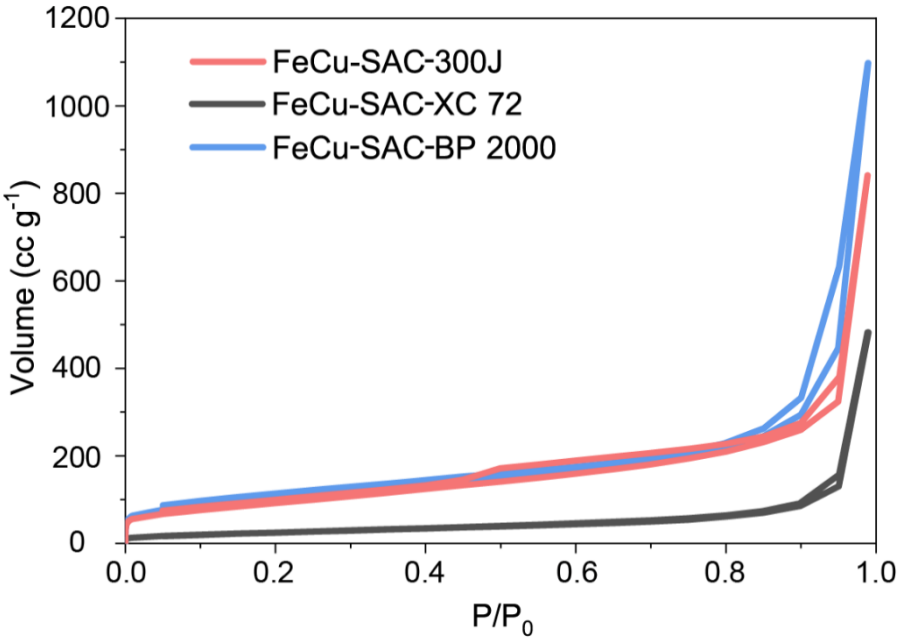

Fig. S29. N_2 adsorption-desorption curves for FeCu-SAC synthesized on different carbon substrates.

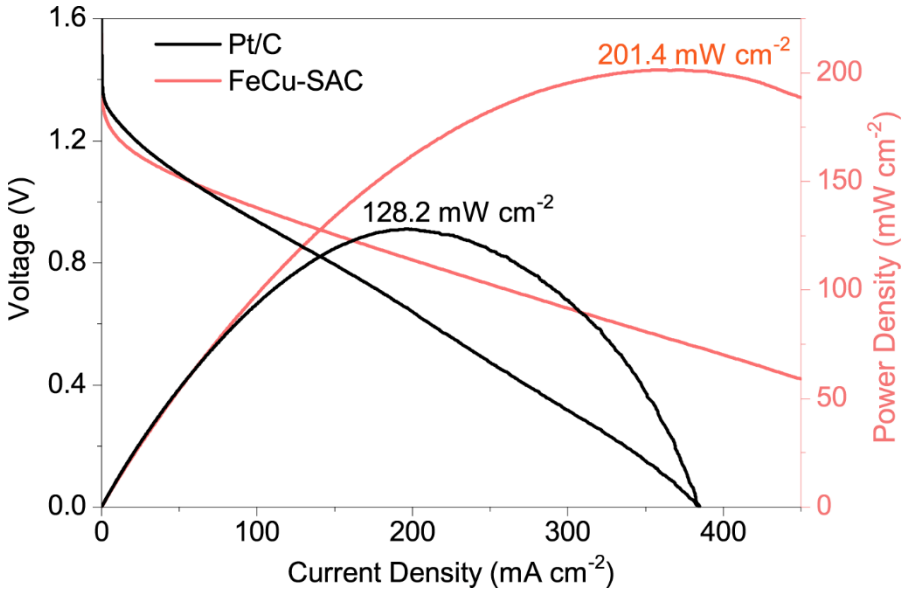

Fig. S30. Discharge polarization curves and the corresponding power density curves of Zn-air batteries constructed by FeCu-SAC and Pt/C.

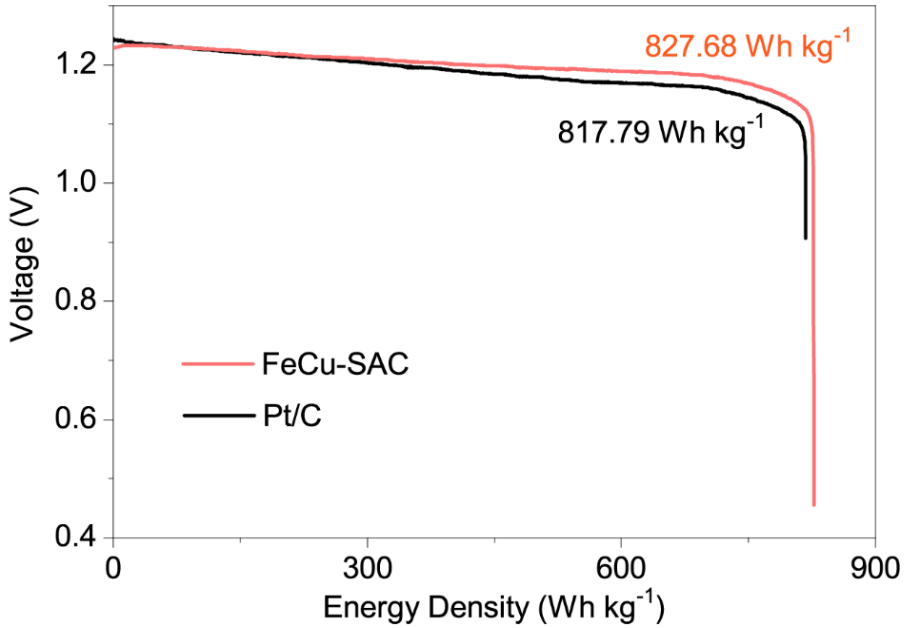

Fig. S31. Galvanostatic discharge curves of Zn-air batteries constructed by FeCu-SAC and Pt/C at a current density of 20 mA cm^{-2}.

Table S1. Fitting results for FeCu-SAC.

Sample	Path	N	R (Å)	σ^2 (Å)	ΔE_0 (eV)	R factor
Fe foil[a]	Fe-Fe	8	2.46	0.00468	5.833	0.0065
	Fe-Fe	6	2.85	0.00527	5.728	
Cu foil[b]	Cu-Cu	12	2.54	0.00861	4.562	0.0017
FeCu-SAC[c]	Fe-N	3.8	2.01	0.00574	5.59	0.011
	Cu-N	4.06	1.99	0.00572	1.272	0.022

[a]: k range: 3-10.0 ($Å^{-1}$); R range: 1-3 Å; S_0 = 0.687 [b]: k range: 2.7-13.6 ($Å^{-1}$); R range: 1.15-3 Å; S_0 = 0.837; S_0 = 0.837 [c]: k range: 2.59-8.18 ($Å^{-1}$); R range: 1.15-3.58 Å for Fe-N path. k range: 2.3-9.0 ($Å^{-1}$); R range: 0.8-3.0 Å for Cu-N path.

Table S2. The contents of different N type in FeCu-SAC, Fe-SAC and Cu-SAC.

sample	N content %	Pyridinic N percentage %	Pyrrolic N percentage %	Graphitic N percentage %	Oxidized N percentage %
FeCu-SAC	2.66	43.86	19.57	19.67	16.91
Fe-SAC	1.97	44.06	15.30	17.62	23.01
Cu-SAC	2.23	40.90	23.98	14.70	20.41

Table S3. Comparison of dual metal single atom catalysts for ORR in alkaline condition.

Name	Half-wave potential (V)	Kinetic current density	Tafel slope (mV dec^{-1})	Ref.
FeCu-SAC	0.926	16.33 mA cm^{-2} at 0.9 V	53.6	This work
FeCu-DA/NC	0.860	1.87 mA cm^{-2} at 0.85 V	57	[8]
Cu-Fe-N-C	0.864	/	100.1	[9]
Cu@Fe-N-C	0.892	/	78	[10]
FeCu-NC	0.882	14.78 mA cm^{-2} at 0.85 V	74	[11]
NCAG/Fe-Cu	0.940	25.5 mA cm^{-2} at 0.85 V	55	[12]
Fe_1Co_3-NC-1100	0.877	/	69.06	[13]
CoFe-NC-900	0.940	/	68	[14]
Co_2/Fe-N@CHC	0.915	9.44 mA cm^{-2} at 0.90 V	62	[15]
f-FeCoNC900	0.890	/	/	[16]
CoFe-N-C	0.897	/	/	[17]
Ni-N_4/GHSs/Fe-N_4	0.830	/	55	[18]
FeNi SAs/NC	0.840	/	54.68	[19]
Fe/Mn-Nx-C	0.880	13.58 mA cm^{-2} at 0.85 V	/	[20]
FeMn-DSAC	0.922	27.0 mA cm^{-2} at 0.90 V	33	[21]
Fe_1Se_1-NC	0.880	/	/	[22]
Fe-N_4/Pt-N_4@NC	0.930	27.2 mA cm^{-2} at 0.85 V	78	[23]
COF@MOF_{800}-Fe	0.890	/	80	[24]
Cu/Zn-NC	0.830	/	54.8	[25]

References

[1] Kresse, G. Furthmuller, J. *Phys. Rev. B Condens. Matter.,* **1996,** 54, 11169-11186

[2] Hammer, B., Hansen, L. B.Norskov, J. K., *Phys. Rev. B,* **1999,** 59, 7413-7421

[3] Ernzerhof, M. Scuseria, G. E., *J. Chem. Phys.,* **1999,** 110, 5029-5036

[4] Huang, H., Wu, H.-H., Chi, C., Huang, B.Zhang, T.-Y., *J. Mater. Chem. A,* **2019,** 7, 8897-8904

[5] Li, J., Huang, H., Cao, X., Wu, H.-H., Pan, K., Zhang, Q., Wu, N.Liu, X., *Chem. Eng. J.,* **2021,** 416, 127677

[6] Grimme, S., Antony, J., Ehrlich, S.Krieg, H., *J. Chem. Phys.,* **2010,** 132, 154104

[7] Wang, V., Xu, N., Liu, J.-C., Tang, G.Geng, W.-T., *Computer Phys. Commun.,* **2021**, 108033

[8] Du, C., Gao, Y., Chen, H., Li, P., Zhu, S., Wang, J., He, Q.Chen, W., *J. Mater. Chem. A,* **2020,** 8, 16994-17001

[9] Li, J., Chen, J., Wan, H., Xiao, J., Tang, Y., Liu, M.Wang, H., *Appl. Catal., B,* **2019,** 242, 209-217

[10] Wang, Z., Jin, H., Meng, T., Liao, K., Meng, W., Yang, J., He, D., Xiong, Y.Mu, S., *Adv. Funct. Mater.,* **2018,** 28, 1802596

[11] Xiao, Z., Sun, P., Qiao, Z., Qiao, K., Xu, H., Wang, S.Cao, D., *Chem. Eng. J.,* **2022,** 446, 137112

[12] He, T., Chen, Y., Liu, Q., Lu, B., Song, X., Liu, H., Liu, M., Liu, Y. N., Zhang, Y., Ouyang, X.Chen, S., *Angew. Chem., Int. Ed.,* **2022,** 61, e202201007

[13] He, Y. T., Yang, X. X., Li, Y. S., Liu, L. T., Guo, S. W., Shu, C. Y., Liu, F., Liu, Y. N., Tan, Q.Wu, G., *ACS Catal.,* **2022,** 12, 1216-1227

[14] Wang, K., Liu, J. P., Tang, Z. H., Li, L. G., Wang, Z., Zubair, M., Ciucci, F., Thomsen, L., Wright, J.Bedford, N. M., *J. Mater. Chem. A,* **2021,** 9, 13044-13055

[15] Wang, Z., Jin, X., Zhu, C., Liu, Y., Tan, H., Ku, R., Zhang, Y., Zhou, L., Liu, Z., Hwang, S. J.Fan, H. J., *Adv. Mater.,* **2021,** 33, e2104718

[16] Zhang, G. X., Jia, Y., Zhang, C., Xiong, X. Y., Sun, K., Chen, R. D., Chen, W. X., Kuang, Y., Zheng, L. R., Tang, H. L., Liu, W., Liu, J. F., Sun, X. M., Lin, W.

F.Dai, H. J., *Energy Environ. Sci.,* **2019,** 12, 1317-1325

[17] Zhou, X. Y., Gao, J. J., Hu, Y. X., Jin, Z. Y., Hu, K. L., Reddy, K. M., Yuan, Q. H., Lin, X.Qiu, H. J., *Nano Lett.,* **2022,** 22, 3392-3399

[18] Chen, J., Li, H., Fan, C., Meng, Q., Tang, Y., Qiu, X., Fu, G.Ma, T., *Adv. Mater.,* **2020,** 32, e2003134

[19] Yu, D. S., Ma, Y. C., Hu, F., Lin, C. C., Li, L. L., Chen, H. Y., Han, X. P.Peng, S. J., *Adv. Energy Mater.,* **2021,** 11, 2101242

[20] Chen, Z., Liao, X. B., Sun, C. L., Zhao, K. N., Ye, D. X., Li, J. T., Wu, G., Fang, J. H., Zhao, H. B.Zhang, J. J., *Appl. Catal., B,* **2021,** 288, 120021

[21] Cui, T., Wang, Y. P., Ye, T., Wu, J., Chen, Z., Li, J., Lei, Y., Wang, D.Li, Y., *Angew. Chem., Int. Ed.,* **2022**, e202115219

[22] Chen, Z., Su, X., Ding, J., Yang, N., Zuo, W., He, Q., Wei, Z., Zhang, Q., Huang, J.Zhai, Y., *Appl. Catal., B,* **2022,** 308, 121206

[23] Han, A., Wang, X. J., Tang, K., Zhang, Z. D., Ye, C. L., Kong, K. J., Hu, H. B., Zheng, L. R., Jiang, P., Zhao, C. X., Zhang, Q., Wang, D. S.Li, Y. D., *Angew. Chem., Int. Ed.,* **2021,** 60, 19262-19271

[24] Miao, Q., Yang, S., Xu, Q., Liu, M., Wu, P., Liu, G., Yu, C., Jiang, Z., Sun, Y.Zeng, G., *Small Struct.,* **2022,** 3, 2100225

[25] Tong, M., Sun, F., Xie, Y., Wang, Y., Yang, Y., Tian, C., Wang, L.Fu, H., *Angew. Chem., Int. Ed.,* **2021,** 60, 14005-14012